Megahertz dynamics in skyrmion systems probed with muon-spin relaxation

T. J. Hicken,[1] M. N. Wilson,[1] K. J. A. Franke,[1,*] B. M. Huddart,[1] Z. Hawkhead,[1] M. Gomilšek,[1,†] S. J. Clark,[1] F. L. Pratt,[2] A. Štefančič,[3,‡] A. E. Hall,[3] M. Ciomaga Hatnean,[3] G. Balakrishnan,[3] and T. Lancaster[1]

[1]*Centre for Materials Physics, Durham University, Durham DH1 3LE, United Kingdom*

[2]*ISIS Pulsed Neutron and Muon Facility, STFC Rutherford Appleton Laboratory, Harwell Oxford, Didcot OX11 OQX, United Kingdom*

[3]*Department of Physics, University of Warwick, Coventry CV4 7AL, United Kingdom*

(Received 18 September 2020; revised 20 November 2020; accepted 14 December 2020; published 19 January 2021)

We present longitudinal-field muon-spin relaxation (LF μSR) measurements on two systems that stabilize a skyrmion lattice (SkL): Cu_2OSeO_3, and $Co_xZn_yMn_{20-x-y}$ for $(x, y) = (10, 10)$, $(8, 9)$, and $(8, 8)$. We find that the SkL phase of Cu_2OSeO_3 exhibits emergent dynamic behavior at megahertz frequencies, likely due to collective excitations, allowing the SkL to be identified from the μSR response. From measurements following different cooling protocols and calculations of the muon stopping site, we suggest that the metastable SkL is not the majority phase throughout the bulk of this material at the fields and temperatures where it is often observed. The dynamics of bulk $Co_8Zn_9Mn_3$ are well described by $\simeq$2 GHz excitations that reduce in frequency near the critical temperature, while in $Co_8Zn_8Mn_4$ we observe similar behavior over a wide range of temperatures, implying that dynamics of this kind persist beyond the SkL phase.

DOI: 10.1103/PhysRevB.103.024428

I. INTRODUCTION

The skyrmion has received the attention of much recent research [1,2] due to its potential for future spintronic applications [3,4]. Several mechanisms can lead to the stabilization of a skyrmion spin texture, with examples in thin films, multilayer stacks, and bulk materials [1,2]; the region of stability of the skyrmion phase in the B-T phase diagram is quite different in different systems (Fig. 1) [5–17]. For applications it is important to understand the spin dynamics of skyrmions, which are most commonly studied in systems which host a skyrmion lattice (SkL). Originally detected using microwave spectroscopy techniques in Cu_2OSeO_3 [18], three modes in the GHz regime are identified as excitations of the Bloch skyrmion: counterclockwise, breathing, and clockwise modes [19]. In addition, some SkL-hosting materials show other collective excitations, e.g., THz excitations in Cu_2OSeO_3 due to spin excitations in high-energy magnon bands [20–23].

In general, ordered magnets host diffusive and propagating magnetic excitations; we therefore expect excitations over a wide range of frequencies. Despite this, there are few reports on the excitation spectra of SkL-hosting materials in the MHz regime. One technique that can probe this regime, which is sensitive to dynamics of the internal magnetic field, is longitudinal-field muon-spin relaxation (LF μSR). LF μSR is a technique with a unique time window, sensitive to dynamics between approximately 10 kHz and 1 THz [24]. It has been applied previously to exponentially correlated fluctuations of the dense array of moments found in typical magnetic materials [24] and to more complex dynamic behavior such as diffusive and ballistic transport in spin chains [25,26], correlated fluctuations in metallic ferromagnets [27], and soliton motion in polymers [28]. However, only a handful of results have been reported where LF μSR is used to study the skyrmion lattice (SkL). Studied systems include $Cu_{2-x}Zn_xOSeO_3$ [29] (which hosts Bloch skyrmions) and $GaV_4S_{8-y}Se_y$ [30,31] (which hosts Néel skyrmions). Similar behavior is observed in these materials, with an enhanced and broadened peak in the muon-spin relaxation rate found at temperatures just below the critical temperature T_c at those external magnetic fields that stabilize the SkL.

Here we investigate the LF μSR response in two materials that host a Bloch SkL. We study two different systems with contrasting crystal symmetries in which the noncentrosymmetric crystal structure leads to a bulk Dzyaloshinskii-Moriya interaction, thus stabilizing the SkL through competition with symmetric exchange. The first is Cu_2OSeO_3 [8], an insulating, multiferroic ferrimagnet which crystallizes in the $P2_13$ structure. The stability and extent of the skyrmion lattice in Cu_2OSeO_3 can be controlled both with an externally applied electric field (E field) [32] and through chemical substitution of the magnetic Cu ions [33]. The second is $Co_xZn_yMn_{20-x-y}$ [9], which is a metallic system with the β-Mn structure, known for its chemical substitutional site disorder. The magnetic properties of the system change significantly with x and y, and the series is of particular interest in those compositions that host a SkL above room temperature. In both systems we are able to use muons to observe a dynamic response on the MHz timescale that is unique to fields which stabilize the SkL.

The paper is structured as follows: in Sec. II we describe the experimental and analytical procedures used; in

*Present address: School of Physics and Astronomy, University of Leeds, Leeds LS2 9JT, United Kingdom.

†Present address: Jožef Stefan Institute, Jamova c. 39, SI-1000 Ljubljana, Slovenia.

‡Present address: Electrochemistry Laboratory, Paul Scherrer Institut, CH-5232 Villigen PSI, Switzerland.

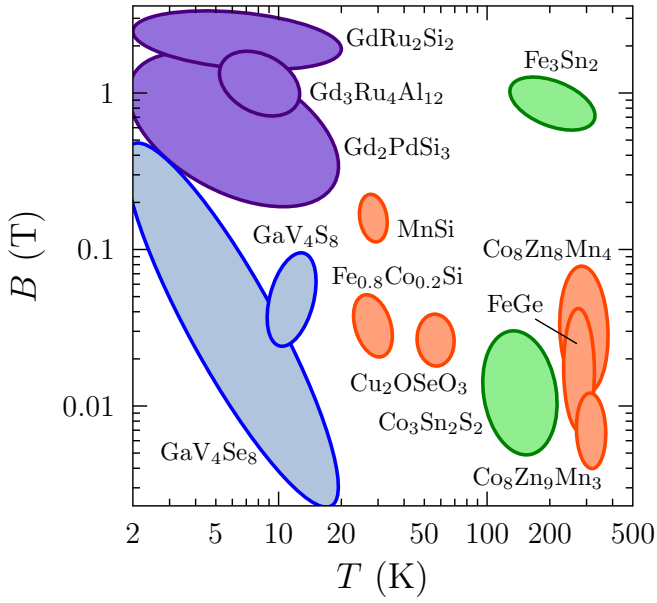

FIG. 1. Skyrmion phase diagram of bulk materials. Stabilization of the skyrmion phase occurs through various mechanisms: (i) competition between the exchange and Dzyaloshinskii-Moriya interactions, leading to a Bloch (orange) or Néel (blue) skyrmion lattice, (ii) competition between exchange and uniaxial anisotropy (green), (iii) geometric frustration from the interplay of Ruderman-Kittel-Kasuya-Yosida (RKKY) and four-spin interactions (purple). Phase boundaries are taken from Refs. [5–17].

Sec. III we first probe Cu_2OSeO_3 with μSR and analyze the results with support from density functional theory (DFT) calculations of the muon stopping site, before turning to $Co_xZn_yMn_{20-x-y}$, where we present muon stopping site calculations and investigate three different compositions. Additional details can be found in the Supplemental Material [34].

II. EXPERIMENT

Cu_2OSeO_3 samples were synthesized as detailed in Ref. [29], and polycrystalline $Co_xZn_yMn_{20-x-y}$ boules were synthesized as detailed in the Supplemental Material [34]. In a LF μSR experiment spin-polarized positive muons are implanted in a sample in the presence of an external magnetic field parallel to the initial muon-spin direction [34,35]. Implanted muons interact with the local magnetic field at the muon site, which is a sum of the external and internal fields. By measuring the decay of the polarization of the spin of the muon ensemble, one reveals information about both the static and dynamic properties of the local magnetism at the muon site. In the fast-fluctuation regime, typical for an ordered magnet, this relaxation is exponential with a relaxation rate

$$\lambda = \frac{2\Delta^2\nu}{\omega_0^2 + \nu^2}, \tag{1}$$

where ν is the characteristic frequency of the field fluctuations, $\Delta = \gamma_\mu\sqrt{\langle B^2\rangle}$ is the amplitude of the field fluctuations, and $\omega_0 = \gamma_\mu B_{\rm ext}$ is the precession frequency of a muon with gyromagnetic ratio $\gamma_\mu = 2\pi \times 135.5$ MHz T^{-1} in the external field $B_{\rm ext}$. The fluctuations themselves can be described by a spectral density $J(\omega)$, which represents the Fourier transform of the autocorrelation function of the magnetic field at the muon site(s). In cases where $J(\omega)$ is broad in frequency, the muon spin polarization will be most effectively relaxed by the part of the spectral density at frequencies close to $\omega_0 = \gamma_\mu B_{\rm ext}$, which typically lies in the MHz regime for values of $B_{\rm ext}$ applied in our measurements. Detailed information on the experimental procedures employed in this paper can be found in the Supplemental Material [34,36–38].

III. RESULTS AND DISCUSSION

A. Cu_2OSeO_3

LF μSR measurements on a mosaic of single-crystals of Cu_2OSeO_3 were performed upon warming, after cooling in zero applied magnetic field (ZFC). Temperature scans were performed at $B_{\rm ext} = 22$ mT, which stabilizes the SkL state between $\approx$56 K and $\approx$58 K, and at $B = 40$ mT, which does not stabilize a SkL at any temperature [Fig. 2(a)]. Example spectra are shown in Fig. 2(b), where the asymmetry decays monotonically, with an exponential decay typical of relaxation due to the dynamics of a dense array of fluctuating local moments. The spectra are well described at all measured temperatures using a relaxation function

$$A(t) = a_{\rm r}e^{-\lambda t} + a_{\rm b}, \tag{2}$$

where the component with amplitude $a_{\rm r}$ captures the contribution from muons stopping in the sample with their spin initially aligned along the local magnetic field, and the baseline amplitude $a_{\rm b}$ accounts for muons that stop outside of the sample or at positions in the material where a fluctuating field does not dephase them. The relaxing amplitude $a_{\rm r}$ increases as the temperature is raised through the ordering temperature $T_{\rm c}$. To model this, we constrain $a_{\rm r}$ to

$$a_{\rm r} = a_{\rm r}^0 + L[1 + e^{-k(T-T_{\rm c})}]^{-1}, \tag{3}$$

where $a_{\rm r}^0$ is the relaxing amplitude for $T \ll T_{\rm c}$, L is difference between the maximum and minimum relaxing amplitude, and k is a parameter which defines the rate of increase of $a_{\rm r}$ around $T_{\rm c}$. This allows us to extract $T_{\rm c}$ independently of λ. (Extracted values of $T_{\rm c}$ agree well with those from AC susceptibility.) There is no temperature dependence to $a_{\rm b}$, leaving only λ [Fig. 2(c)] varying in our fits.

There are striking differences in the behavior of λ between the two temperature scans. On scanning through the fields in the B-T phase diagram where the SkL is realized, λ is significantly enhanced at those temperatures where the SkL phase is found, resulting in a broad shoulder above 56.5 K that terminates in a peak on the high temperature side. No such enhancement is observed at higher fields. This indicates significantly enhanced $J(\omega)$ around $\omega_0 = 2\pi \times 3$ MHz in the SkL phase and is similar to the behavior previously reported for both the Bloch and Néel-type SkL [29,31]. Therefore, we conclude that LF μSR has a characteristic response to the SkL, specifically an increase in relaxation rate compared to the surrounding magnetic phases.

As variation in the amplitude of the fluctuating field Δ/γ_μ is likely to follow the magnetization, the variation in λ likely

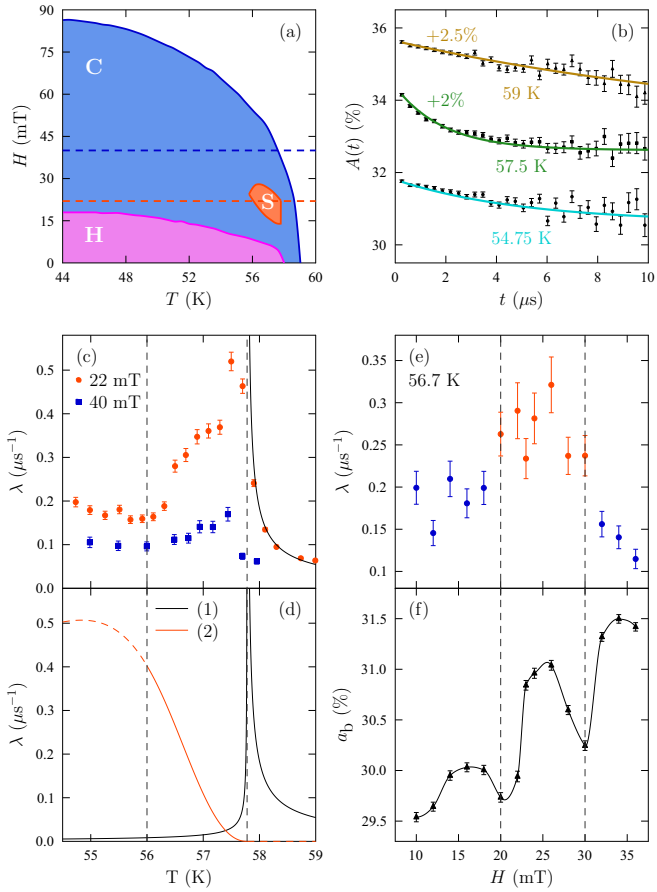

FIG. 2. (a) Phase diagram of Cu_2OSeO_3, showing conical (C), helical (H), and skyrmion (S) phases, reproduced from Ref. [29]. Orange color: fields at which the SkL is stabilized; blue: fields which only stabilize C order below T_c; and pink: H order. (b) Example LF μSR spectra for Cu_2OSeO_3 measured in $B = 22$ mT. For clarity, some data are shown with vertical offsets. (c) Extracted values of λ. (d) Simulations of contributions to λ due to (1) critical slowing down of magnetic fluctuations near T_c (black solid line); (2) reduction in frequency of GHz spectral density (orange solid line). The orange dashed line indicates the value of λ one would obtain if the SkL was stabilized at those temperatures. Vertical dashed lines indicate the location of the SkL at 22 mT from AC susceptibility. (e) Extracted values of λ from a field scan at $T = 56.7$ K, with (f) accompanying baseline amplitude (the solid line is a guide to the eye). Dashed lines indicate the location of the SkL at 56.7 K.

results from the temperature dependence of ν, and could reflect (1) critical slowing down of the magnetic fluctuations near T_c, typical of a second-order phase transition; (2) reduction in frequency of the skyrmion excitation modes near T_c; (3) other collective dynamics of the system occurring on the MHz timescale.

(1) Above T_c, the relaxation rate λ is well described by power-law behavior [39] typical of critical fluctuations in a three-dimensional (3D) Heisenberg magnet [40–43] with a fluctuation time $1/\nu \propto |T - T_c|^{-w'}$ with $w' = 0.709$, typical for a 3D Heisenberg magnet. Below T_c the same critical parameters do not account for λ, which should show a sharp rise very close to T_c [Fig. 2(d)].

(2) The skyrmion rotational and breathing modes are expected to broaden and decrease in frequency (or soften) as T approaches T_c from below (see, for example, Ref. [33]), contributing to the spectral weight $J(\omega)$ centered around $\omega_0 = \gamma_\mu B_{ext}$ ($2\pi \times 3$ MHz at our value B_{ext}). Assuming that the time-dependent magnetization that results from skyrmion modes determines the relaxation, we can use typical exponents for a 3D Heisenberg model to predict

$$\lambda = \frac{2\Delta_0^2 \nu_0 [1 - (T/T_c)^{3/2}]^{0.73} (1 - T/T_c)^{1.43}}{\gamma_\mu^2 B_{ext}^2 + \nu_0^2 (1 - T/T_c)^{2.86}}. \quad (4)$$

Cu_2OSeO_3 exhibits its lowest frequency skyrmion mode (counterclockwise rotational) at $\nu_0 = 2.3$ GHz [44], giving the behavior shown in Fig. 2(d), which does not describe the measured data. Note that $\nu_0 = 10$–20 GHz would be a better match to the data, but this is at least a factor of 3–4 higher than the three lowest energy modes of the SkL in Cu_2OSeO_3 [44], but too low in frequency to be the THz excitations previously observed.

(3) Alternatively, λ could reflect the occurrence of other low-energy, collective excitations emerging from the SkL involving individual skyrmions or from motion of the SkL (e.g., diffusive excitations resulting when the SkL undergoes collective motion, or where individual skyrmions are created or destroyed). This is plausible given that diffusive dynamics for single skyrmions [45,46] typically occur in the GHz regime, while the motion of Bloch points along skyrmion tubes are likely to occur at MHz frequencies. It could also be that Δ increases near the transition owing to rapid changes in width of the local field distribution at the muon sites. In each of these cases a change in the distribution of skyrmions in the SkL is required.

To further investigate the response to the SkL, LF μSR measurements were also made as a function of increasing applied magnetic field B at fixed temperature $T = 56.7$ K after ZFC. These data are also well described by Eq. (2), with a field-independent amplitude a_r and a baseline a_b that increases with B, as is often observed in LF μSR. We again observe enhanced values of λ in the SkL phase, along with discontinuous behavior in a_b marking the transitions in and out of the SkL phase [Figs. 2(e) and 2(f)], providing another method of identifying the SkL phase boundaries. A likely explanation of the observed behavior comes from demagnetization effects, which are known to cause the magnetic transition in and out of the SkL state to occur at slightly different fields for different parts of the sample [47]. This leads to increased disorder in the field distribution at the muon sites, resulting in fewer muons stopping with their spin parallel to the local field, and hence dephasing too rapidly to be observed resulting in a loss of the total, and hence baseline, asymmetry.

We now discuss the internal field distribution, muon sites, and the possibility of observing metastable skyrmions in Cu_2OSeO_3. We performed TF μSR measurements on a single crystal of Cu_2OSeO_3 after ZFC and rapid cooling in an applied field (FC) ($\approx$17 K/minute). This rapid FC is expected to stabilize metastable skyrmions at temperatures that host a conical phase for ZFC [33]. TF measurements are sensitive to the static internal magnetic field distribution of the sample at the muon sites, and has been shown to be sensitive to changes

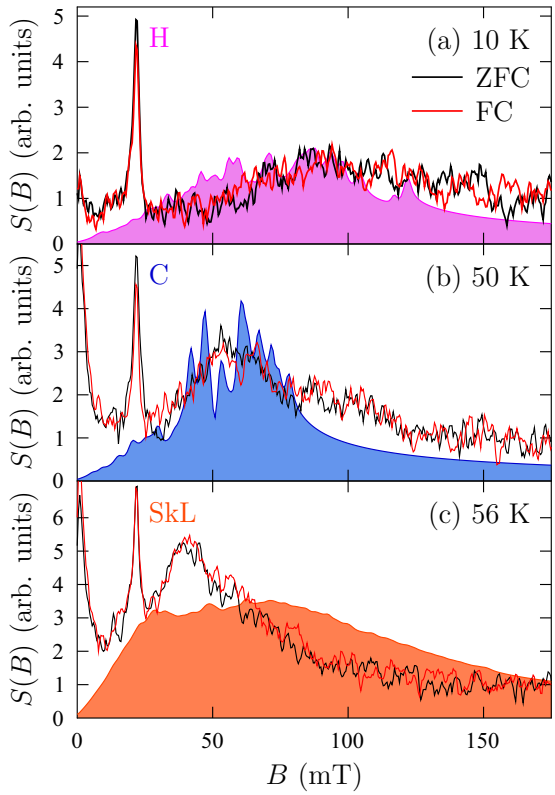

FIG. 3. Internal magnetic field distributions [$S(B)$] of Cu_2OSeO_3 at various T measured by TF μSR for $B_{ext} = 22$ mT, with comparison to simulations. Black lines: measurements performed after ZFC; red lines: after rapid FC (≈17 K/minute); solid color: simulated distributions for different spin structures.

in the magnetic state in this material [48]. Internal field distributions derived from TF measurements measured after both ZFC and rapid FC are compared in Fig. 3 in an applied field of 22 mT. There is a characteristic change in distributions for the different magnetic states [48], which are observed after both field protocols, but no significant difference is observed between the two protocols, suggesting that the local field distribution is similar in both cases. (The peak observed at 22 mT at all temperatures occurs from muons stopping outside of the sample and precessing in the applied field.)

To model magnetic field distributions for the ordered states in Cu_2OSeO_3, muon stopping sites were determined using DFT methods to relax the structure with an implanted muon [34,49–52]. We find different sites than those identified in Ref. [53], which were determined by finding the minima of the unperturbed electrostatic potential in the crystal with no muon present. Our three distinct sites (of which only the two lowest energy are found to be occupied) are shown in Table I, with simulated field distributions at the muon sites shown in Fig. 3 (for further details see [34,48,54–57]). The simulations describe the experimental results reasonably well, with the worst match being for the SkL where, with increasing field, the rapid increase followed by slow decrease of spectral weight is captured, but the absolute values do not agree closely. The good match between simulation and experiment in the helical and conical states shows that the static magnetism in these phases is sufficient to describe the

TABLE I. Calculated muon stopping sites in Cu_2OSeO_3. Energies are given relative to the lowest energy site.

Muon site	Fractional coordinates	Energy (eV)
1	(0.906, 0.590, 0.100)	0.00
2	(0.172, 0.365, 0.319)	0.09
3	(0.224, 0.670, 0.289)	0.15

response on the muon timescale. The greater discrepancy between simulation and experiment in the SkL state provides further evidence, independently of the LF μSR, that there is a significant dynamic effect on the muon timescale which affects the internal magnetic field distribution of the sample. The lack of difference in the distributions observed after ZFC and FC protocols indicates that the metastable SkL is not the majority phase through the entire sample [34]. This could suggest that the metastable SkL is more likely to exist in particular parts of a sample, such as sample edges or defects. A propensity for skyrmions to form near surfaces would also explain the lack of any muon signal, since the muons penetrate several microns into the sample in the measurements.

Another potential way to manipulate the SkL density in Cu_2OSeO_3 is through the application of an E field whose orientation and magnitude causes the SkL phase to exist over different T ranges [32]. We performed LF μSR on a polycrystalline pellet of Cu_2OSeO_3 with an E field applied parallel/antiparallel to the externally applied magnetic field B_{ext} [34]. Similarly, we find that in those cases where the SkL is not the majority phase its dynamic signature is not resolved, making it likely that μSR is sensitive to the SkL in this system only when it is the majority volume phase.

B. $Co_xZn_yMn_{20-x-y}$

We now turn to the $Co_xZn_yMn_{20-x-y}$ system with $(x, y) = (10, 10)$, (8, 9), and (8, 8). Some members of the $Co_xZn_yMn_{20-x-y}$ series host a SkL at or above room temperature, making the series potentially favorable for future applications. However, crystallographic site disorder inherent in these materials presents challenges, such as the broadening, both in temperature and applied field, of the magnetic transitions due to locally different crystallographic environments throughout the sample, and dramatic effects on T_c with relatively subtle changes in composition [58]. By studying these three materials we can consider the effect of increasing site disorder (which mainly occurs on the 12d Wyckoff site) on the magnetism. The level of disorder increases with decreasing y until, once $y \lesssim 7$, a spin glass ground state is realized [59]. Here we study the regime where the system remains magnetically ordered.

The muon stopping sites in $Co_{10}Zn_{10}$, $Co_8Zn_9Mn_3$, and $Co_8Zn_8Mn_4$ were calculated using DFT [34], with results presented in Table II. The environment of the muon affects its energy, so, due to the significant site disorder, each site has a range of energies (depending on the atoms near the site for the particular simulated structure). This will affect which sites are occupied.

We first consider the LF μSR response of the parent compound, $Co_{10}Zn_{10}$, which has not been reported to

TABLE II. Calculated muon stopping sites in $Co_xZn_yMn_{20-x-y}$. Typical energies of the site are given relative to the lowest energy site. The ranges reflect the fact that the local environment of each site affects the energy. For sites 2 and 3 the energy ranges only apply for 20% Mn concentration and below; above this concentration the sites are not realized in the calculations.

Muon site	Fractional coordinates	Typical energy range (eV)
1	(0.179, 0.571, 0.319)	0.00–0.98
2	(0.344, 0.398, 0.337)	0.31–1.03
3	(0.426, 0.568, 0.073)	0.42–0.97

stabilize a SkL. Exponential decay of the asymmetry is seen at all measured temperatures and magnetic fields. A weak, temperature-independent relaxation is observed on the baseline with a rate consistent with Ag [$\lambda_b = 0.0026(2)\ \mu s^{-1}$]. The data are fitted to the function

$$A(t) = a_r e^{-\lambda t} + a_b e^{-\lambda_b t}. \quad (5)$$

The relaxing amplitude is again constrained to follow Eq. (3) and the resulting relaxation rate λ is shown in Fig. 4(a). We find that measurements at two longitudinal fields have similar temperature dependence, with the overall shape of λ reminiscent of that measured for Cu_2OSeO_3 at 40 mT [Fig. 2(c)], i.e., outside the skyrmion phase, where there is also a transition from the conical to paramagnetic phase. There is no evidence for any additional dynamics at either field, with the sharp peak likely occurring due to critical slowing down of the magnetic fluctuations as the phase transition from the conical to paramagnetic phase is approached [cf. Fig. 2(d)].

Next we discuss $Co_8Zn_9Mn_3$, a composition which can stabilize not only a SkL, but also a meron-antimeron spin texture. Both of these textures have been observed in thin plates [60], with evidence for the SkL in the bulk consisting of magnetization and magnetic entropy measurements [58]. We made measurements in two applied fields: $B_{ext} = 10$ mT, which stabilizes a SkL just below T_c in bulk samples ($321 \lesssim T \lesssim 326$ K), and 18 mT, which gives a field-polarized magnetic state. The spectra decay exponentially at all temperatures and fields and are fitted using the same method as above, with λ shown in Fig. 4(b). The temperature dependence of λ is different from that found in $Co_{10}Zn_{10}$: the peak for $Co_8Zn_9Mn_3$ is significantly broadened with the peak in λ occurring significantly below the obtained T_c, with similar behavior seen at both a field that is expected to stabilize the SkL and one that is not. The relaxation rate λ at both fields is well described by Eq. (4) involving coupling to GHz excitations; although we assume 3D Heisenberg scaling parameters, the result is robust with a different choice of parameters. Further, critical behaviors of both Δ and ν are required to well describe the data; critical behavior of one parameter alone cannot describe these data. The fits shown in Fig. 4(b) suggest $\Delta_{T=0} \simeq 0.01$–0.02 mT and $\nu_{T=0} \simeq 2$ GHz, so that this frequency can be identified with the characteristic excitations in this regime. The fitted frequency is very similar to those found for other SkL systems [44] and suggests that there are dynamics occurring over a range of fields with spectral weight that decreases in frequency with increasing temperature, passing through the frequency range that μSR is sensitive to just below T_c. The fits to the model are best above $T \simeq 280$ K, which is far greater in extent than the reported stability region of the SkL in bulk samples, but where the SkL and meron-antimeron states are reported in thin plates [60]. The wide range of fields over which we detect enhanced dynamics in these bulk samples and the contrast in the extent of the SkL in plates might therefore suggest that the decisive mechanism determining the extent of the phase diagram in the thin plate samples of $Co_8Zn_9Mn_3$ is confinement.

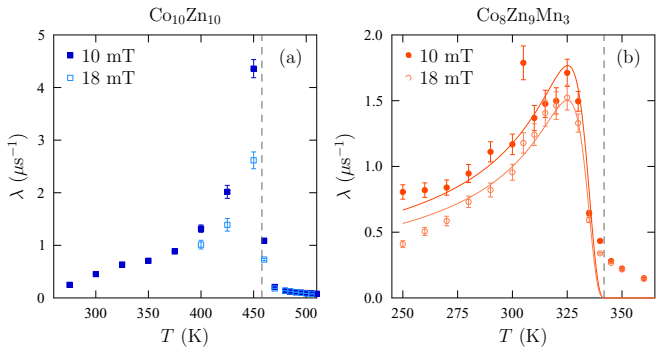

FIG. 4. Extracted values of λ from fitting LF μSR measurements of (a) $Co_{10}Zn_{10}$ and (b) $Co_8Zn_9Mn_3$. The dashed lines indicate the average value of T_c in each sample according to the relaxing amplitude. Fits in (b) are described in the main text.

We now turn to $Co_8Zn_8Mn_4$, which hosts a SkL around room temperature, as shown in Fig. 5(a) [11], with the exact location of the SkL phase dependent on the precise level of Mn present. LF μSR measurements on sample 1 again show exponential relaxation. The same fitting procedure is employed as above, with λ shown in Fig. 5(c). At $B_{ext} = 8$ mT, which is not expected to cut through the SkL, the peak in λ looks typical of previous measurements that do not cut through the SkL, although the peak is well below T_c. The behavior at 26 mT (which does cut through the SkL) is more unusual, with a flattened, broad maximum, and enhanced values of λ observed over a range of temperatures. The suppressed peak at T_c is consistent with different grains of the sample undergoing a transition at slightly different temperatures, caused by slightly varied compositions across parts of the sample. (Mn metal has considerable vapor pressure at 1025 °C, meaning that Mn can migrate toward the surface of the melt during sample synthesis, forming a gradient in composition as observed in Ni_2MnGa [61].)

We find that the enhanced relaxation rate in $Co_8Zn_8Mn_4$ is found at those fields that stabilize the SkL in the *B-T* phase diagram, even at temperatures lower than those that stabilize the SkL state. It is notable both that similar behavior is seen in lightly substituted $GaV_4S_{8-y}Se_y$ [31] and that individual skyrmion formation has been reported in MnSi above T_c at those fields that stabilize the SkL [62]. These three systems, all crystallographically distinct (and, in the case of $GaV_4S_{8-y}Se_y$, hosting a different type of skyrmion), all therefore suggest that the important parameter for skyrmion creation in the Hamiltonian is the applied field, with, as is the current consensus [1,2], thermal fluctuations stabilizing the SkL phase.

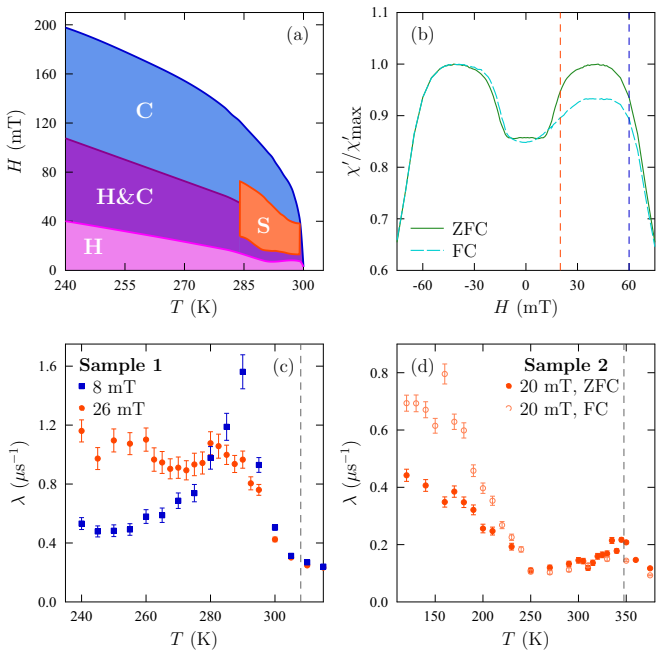

FIG. 5. (a) Representative phase diagram of $Co_8Zn_8Mn_4$, showing helical (H), conical (C), and skyrmion lattice (S) phases, as well as a region of coexistence [11]. (b) AC susceptibility measurements at 250 K after ZFC and FC (in 15 mT) on one sample of $Co_8Zn_8Mn_4$, indicating a metastable SkL after FC. Fields measured with μSR in (d) and Fig. S5 are indicated with dashed lines. (c) and (d) Relaxation rate λ from LF μSR measurements on two different samples, with T_c indicated. In (d) different field protocols are employed.

Finally we consider the effect of a FC protocol in $Co_8Zn_8Mn_4$, which is expected to stabilize a metastable SkL over a wide range of temperature. For these measurements we used a different polycrystalline boule (sample 2). To confirm the existence of the metastable SkL, AC susceptibility measurements were performed and are presented in Fig. 5(b); the suppression of χ', typical of the SkL, is seen over a wide range of fields when employing a FC protocol. LF μSR measurements were performed after both ZFC and FC protocols, with λ shown in Fig. 5(d). The higher value of T_c is likely obtained due to a subtly different composition of sample 2 compared to sample 1 used for these measurements (specifically, we expect that sample 2 is Mn deficient, with the differences between samples likely occurring due to the different dwell times during synthesis as previously discussed).

The data measured at $B_{ext} = 60$ mT (see Supplemental Material [34]) show a peak in λ, typical of those scans that do not cut through the SkL. At 20 mT, where a SkL is formed just below T_c, similar behavior is seen as was found in Fig. 5(c), with a suppressed, flattened peak at T_c for both field protocols. There is, however, an enhanced response in λ at low T for FC compared to ZFC, suggesting that the stabilization of a metastable SkL is affecting the dynamics we observe. Although this contrasts with the results seen for Cu_2OSeO_3, it is consistent with the expected higher stability, and hence increased volume, of the metastable SkL in $Co_8Zn_8Mn_4$ [11,33]. This matches the picture where site disorder allows dynamics similar to those observed in the SkL to persist to lower temperatures, as is the case in $GaV_4S_{8-y}Se_y$ [31]. In this case, stabilization of the metastable SkL likely make the dynamics more prominent, leading to the enhanced λ observed.

IV. CONCLUSION

In Cu_2OSeO_3 high statistics LF μSR measurements reveal complex behavior in the SkL phase, possibly reflecting diffusive excitations of the skyrmion state, either through collective motion or the creation or annihilation of skyrmions. Through TF μSR measurements and calculation of the muon stopping sites in Cu_2OSeO_3 we suggest that the metastable SkL is unlikely to be found throughout the entire sample, and we suggest that it may be more stable at boundaries and surfaces.

A range of behavior is observed in $Co_xZn_yMn_{20-x-y}$. We have shown that there are MHz dynamics in $Co_8Zn_9Mn_3$, regardless of whether the field stabilizes a SkL, that can be well described by a model involving coupling to $\simeq$2 GHz excitations whose frequency drops near T_c. In $Co_8Zn_8Mn_4$ we have shown evidence for enhanced dynamics over a wide range of temperatures when the external field is one that stabilizes the SkL. Stabilization of a metastable SkL enhances these dynamics, likely due to a greater proportion of muons being sensitive to SkL effects. Identifying the precise source of these MHz dynamics in SkL systems, now observed in multiple materials, should be an avenue for future research.

Research data from this paper will be made available via Durham Collections [63].

ACKNOWLEDGMENTS

Part of this work was carried out at the STFC ISIS Facility, UK, and part of this work was carried out at the Swiss Muon Source, Paul Scherrer Institut, Switzerland; we are grateful for the provision of beam time. This work made use of the facilities of the Hamilton HPC Service of Durham University. The project was funded by EPSRC (UK) (Grants No. EP/N032128/1 and No. EP/N024028/1). M.N.W. acknowledges the support of the Natural Sciences and Engineering Research Council of Canada (NSERC). M.G. would like to acknowledge support from the Slovenian Research Agency under project Z1-1852. M.C.H. would like to acknowledge support from EPSRC (UK) under Grant No. EP/T005963/1. We are grateful to B. Nicholson for help with sputtering the electrical contacts on the Cu_2OSeO_3 pellet, and F. Xiao and H. Luetkens for experimental assistance at PSI.

[1] T. Lancaster, Skyrmions in magnetic materials, Contemp. Phys. **60**, 246 (2019).

[2] K. Everschor-Sitte, J. Masell, R. M. Reeve, and M. Kläui, Perspective: Magnetic skyrmions—Overview of recent progress in an active research field, J. Appl. Phys. **124**, 240901 (2018).

[3] G. Finocchio, F. Büttner, R. Tomasello, M. Carpentieri, and M. Kläui, Magnetic skyrmions: from fundamental to applications, J. Phys. D **49**, 423001 (2016).

[4] A. Fert, N. Reyren, and V. Cros, Magnetic skyrmions: advances in physics and potential applications, Nat. Rev. Mater. **2**, 17031 (2017).

[5] S. Mühlbauer, B. Binz, F. Jonietz, C. Pfleiderer, A. Rosch, A. Neubauer, R. Georgii, and P. Böni, Skyrmion lattice in a chiral magnet, Science **323**, 915 (2009).

[6] W. Münzer, A. Neubauer, T. Adams, S. Mühlbauer, C. Franz, F. Jonietz, R. Georgii, P. Böni, B. Pedersen, M. Schmidt *et al.*, Skyrmion lattice in the doped semiconductor $Fe_{1-x}Co_xSi$, Phys. Rev. B **81**, 041203(R) (2010).

[7] H. Wilhelm, M. Baenitz, M. Schmidt, U. K. Rößler, A. A. Leonov, and A. N. Bogdanov, Precursor Phenomena at the Magnetic Ordering of the Cubic Helimagnet FeGe, Phys. Rev. Lett. **107**, 127203 (2011).

[8] S. Seki, X. Z. Yu, S. Ishiwata, and Y. Tokura, Observation of skyrmions in a multiferroic material, Science **336**, 198 (2012).

[9] Y. Tokunaga, X. Z. Yu, J. S. White, H. M. Rønnow, D. Morikawa, Y. Taguchi, and Y. Tokura, A new class of chiral materials hosting magnetic skyrmions beyond room temperature, Nat. Commun. **6**, 7638 (2015).

[10] I. Kézsmárki, S. Bordács, P. Milde, E. Neuber, L. M. Eng, J. S. White, H. M. Rønnow, C. D. Dewhurst, M. Mochizuki, K. Yanai *et al.*, Néel-type skyrmion lattice with confined orientation in the polar magnetic semiconductor GaV_4S_8, Nat. Mater. **14**, 1116 (2015).

[11] K. Karube, J. S. White, N. Reynolds, J. L. Gavilano, H. Oike, A. Kikkawa, F. Kagawa, Y. Tokunaga, H. M. Rønnow, Y. Tokura *et al.*, Robust metastable skyrmions and their triangular–square lattice structural transition in a high-temperature chiral magnet, Nat. Mater. **15**, 1237 (2016).

[12] Z. Hou, W. Ren, B. Ding, G. Xu, Y. Wang, B. Yang, Q. Zhang, Y. Zhang, E. Liu, F. Xu *et al.*, Observation of various and spontaneous magnetic skyrmionic bubbles at room temperature in a frustrated kagome magnet with uniaxial magnetic anisotropy, Adv. Mater. **29**, 1701144 (2017).

[13] S. Bordács, A. Butykai, B. G. Szigeti, J. S. White, R. Cubitt, A. O. Leonov, S. Widmann, D. Ehlers, H.-A. K. von Nidda, V. Tsurkan *et al.*, Equilibrium skyrmion lattice ground state in a polar easy-plane magnet, Sci. Rep. **7**, 7584 (2017).

[14] T. Kurumaji, T. Nakajima, M. Hirschberger, A. Kikkawa, Y. Yamasaki, H. Sagayama, H. Nakao, Y. Taguchi, T. Arima, and Y. Tokura, Skyrmion lattice with a giant topological hall effect in a frustrated triangular-lattice magnet, Science **365**, 914 (2019).

[15] M. Hirschberger, T. Nakajima, S. Gao, L. Peng, A. Kikkawa, T. Kurumaji, M. Kriener, Y. Yamasaki, H. Sagayama, H. Nakao *et al.*, Skyrmion phase and competing magnetic orders on a breathing kagomé lattice, Nat. Commun. **10**, 5831 (2019).

[16] H. C. Wu, P. J. Sun, D. J. Hsieh, H. J. Chen, D. C. Kakarla, L. Z. Deng, C. W. Chu, and H. D. Yang, Observation of skyrmion-like magnetism in magnetic Weyl semimetal $Co_3Sn_2S_2$, Mater. Today Phys. **12**, 100189 (2020).

[17] N. D. Khanh, T. Nakajima, X. Yu, S. Gao, K. Shibata, M. Hirschberger, Y. Yamasaki, H. Sagayama, H. Nakao, L. Peng *et al.*, Nanometric square skyrmion lattice in a centrosymmetric tetragonal magnet, Nat. Nanotechnol. **15**, 444 (2020).

[18] Y. Onose, Y. Okamura, S. Seki, S. Ishiwata, and Y. Tokura, Observation of Magnetic Excitations of Skyrmion Crystal in a Helimagnetic Insulator Cu_2OSeO_3, Phys. Rev. Lett. **109**, 037603 (2012).

[19] T. Schwarze, J. Waizner, M. Garst, A. Bauer, I. Stasinopoulos, H. Berger, C. Pfleiderer, and D. Grundler, Universal helimagnon and skyrmion excitations in metallic, semiconducting and insulating chiral magnets, Nat. Mater. **14**, 478 (2015).

[20] V. P. Gnezdilov, K. V. Lamonova, Y. G. Pashkevich, P. Lemmens, H. Berger, F. Bussy, and S. L. Gnatchenko, Magnetoelectricity in the ferrimagnetic Cu_2OSeO_3: symmetry analysis and Raman scattering study, Low Temp. Phys. **36**, 550 (2010).

[21] K. H. Miller, X. S. Xu, H. Berger, E. S. Knowles, D. J. Arenas, M. W. Meisel, and D. B. Tanner, Magnetodielectric coupling of infrared phonons in single-crystal Cu_2OSeO_3, Phys. Rev. B **82**, 144107 (2010).

[22] M. Ozerov, J. Romhanyi, M. Belesi, H. Berger, J.-P. Ansermet, J. van den Brink, J. Wosnitza, S. A. Zvyagin, and I. Rousochatzakis, Establishing the Fundamental Magnetic Interactions in the Chiral Skyrmionic Mott Insulator Cu_2OSeO_3 by Terahertz Electron Spin Resonance, Phys. Rev. Lett. **113**, 157205 (2014).

[23] J. Romhányi, J. van den Brink, and I. Rousochatzakis, Entangled tetrahedron ground state and excitations of the magnetoelectric skyrmion material Cu_2OSeO_3, Phys. Rev. B **90**, 140404(R) (2014).

[24] A. Yaouanc and P. D. De Reotier, *Muon Spin Rotation, Relaxation, and Resonance: Applications to Condensed Matter* (Oxford University Press, Oxford, 2011).

[25] F. L. Pratt, S. J. Blundell, T. Lancaster, C. Baines, and S. Takagi, Low-Temperature Spin Diffusion in a Highly Ideal $S = \frac{1}{2}$ Heisenberg Antiferromagnetic Chain Studied by Muon Spin Relaxation, Phys. Rev. Lett. **96**, 247203 (2006).

[26] B. M. Huddart, M. Gomilšek, T. J. Hicken, F. L. Pratt, S. J. Blundell, P. A. Goddard, S. J. Kaech, J. L. Manson, and T. Lancaster, Magnetic order and ballistic spin transport in a sine-Gordon spin chain, arXiv:2006.13743.

[27] R. S. Hayano, Y. J. Uemura, J. Imazato, N. Nishida, T. Yamazaki, H. Yasuoka, and Y. Ishikawa, Observation of the $T/(T - T_c)$ Divergence of the μ^+ Spin-Lattice Relaxation Rate in MnSi Near T_c, Phys. Rev. Lett. **41**, 1743 (1978).

[28] R. Risch and K. W. Kehr, Direct stochastic theory of muon spin relaxation in a model for trans-polyacetylene, Phys. Rev. B **46**, 5246 (1992).

[29] A. Stefancic, S. H. Moody, T. J. Hicken, M. T. Birch, G. Balakrishnan, S. A. Barnett, M. Crisanti, J. S. O. Evans, S. J. R. Holt, K. J. A. Franke, P. D. Hatton, B. M. Huddart, M. R. Lees, F. L. Pratt, C. C. Tang, M. N. Wilson, F. Xiao, and T. Lancaster, Origin of skyrmion lattice phase splitting in Zn-substituted Cu_2OSeO_3, Phys. Rev. Mater. **2**, 111402 (2018).

[30] K. J. A. Franke, B. M. Huddart, T. J. Hicken, F. Xiao, S. J. Blundell, F. L. Pratt, M. Crisanti, J. A. T. Barker, S. J. Clark, A. Stefancic, M. C. Hatnean, G. Balakrishnan, and T. Lancaster, Magnetic phases of skyrmion-hosting $GaV_4S_{8-y}Se_y$ ($y = 0$, 2, 4, 8) probed with muon spectroscopy, Phys. Rev. B **98**, 054428 (2018).

[31] T. J. Hicken, S. J. R. Holt, K. J. A. Franke, Z. Hawkhead, A. Stefancic, M. N. Wilson, M. Gomilsek, B. M. Huddart, S. J. Clark, M. R. Lees, F. L. Pratt, S. J. Blundell, G. Balakrishnan, and T. Lancaster, Magnetism and Néel skyrmion dynamics in $GaV_4S_{8-y}Se_y$, Phys. Rev. Res. **2**, 032001 (2020).

[32] J. S. White, I. Levatić, A. A. Omrani, N. Egetenmeyer, K. Prša, I. Živković, J. L. Gavilano, J. Kohlbrecher, M. Bartkowiak, H. Berger *et al.*, Electric field control of the skyrmion lattice in Cu_2OSeO_3, J. Phys.: Condens. Matter **24**, 432201 (2012).

[33] M. T. Birch, R. Takagi, S. Seki, M. N. Wilson, F. Kagawa, A. Stefancic, G. Balakrishnan, R. Fan, P. Steadman, C. J. Ottley, M. Crisanti, R. Cubitt, T. Lancaster, Y. Tokura, and P. D. Hatton, Increased lifetime of metastable skyrmions by controlled doping, Phys. Rev. B **100**, 014425 (2019).

[34] See Supplemental Material at http://link.aps.org/supplemental/10.1103/PhysRevB.103.024428 for information on sample synthesis, further details on the muon-spin relaxation technique, a detailed description of the experiments performed, details on the muon stopping site and local magnetic field calculations, and additional muon-spin experiments.

[35] S. J. Blundell, Spin-polarized muons in condensed matter physics, Contemp. Phys. **40**, 175 (1999).

[36] F. L. Pratt, WiMDA: A muon data analysis program for the Windows PC, Phys. B: Condens. Matter **289**, 710 (2000).

[37] F. James and M. Roos, Minuit: A system for function minimization and analysis of the parameter errors and corrections, Comput. Phys. Commun. **10**, 343 (1975).

[38] iminuit team, iminuit–a Python interface to Minuit, https://github.com/scikit-hep/iminuit, accessed 18-05-2020.

[39] F. L. Pratt, P. J. Baker, S. J. Blundell, T. Lancaster, M. A. Green, and M. Kurmoo, Chiral-Like Critical Behavior in the Antiferromagnet Cobalt Glycerolate, Phys. Rev. Lett. **99**, 017202 (2007).

[40] A. Pelissetto and E. Vicari, Critical phenomena and renormalization-group theory, Phys. Rep. **368**, 549 (2002).

[41] E. A. Pospelov, V. V. Prudnikov, P. V. Prudnikov, and A. S. Lyakh, Non-equilibrium critical behavior of the 3D classical Heisenberg model, J. Phys.: Conf. Ser. **1163**, 012020 (2019).

[42] I. Živković, J. S. White, H. M. Rønnow, K. Prša, and H. Berger, Critical scaling in the cubic helimagnet Cu_2OSeO_3, Phys. Rev. B **89**, 060401(R) (2014).

[43] M. N. Wilson, M. T. Birch, A. Štefančič, A. C. Twitchett-Harrison, G. Balakrishnan, T. J. Hicken, R. Fan, P. Steadman, and P. D. Hatton, Stability and metastability of skyrmions in thin lamellae of Cu_2OSeO_3, Phys. Rev. Res. **2**, 013096 (2020).

[44] M. Garst, J. Waizner, and D. Grundler, Collective spin excitations of helices and magnetic skyrmions: review and perspectives of magnonics in non-centrosymmetric magnets, J. Phys. D **50**, 293002 (2017).

[45] J. Miltat, S. Rohart, and A. Thiaville, Brownian motion of magnetic domain walls and skyrmions, and their diffusion constants, Phys. Rev. B **97**, 214426 (2018).

[46] M. Weißenhofer and U. Nowak, Diffusion of skyrmions: The role of topology and anisotropy, New J. Phys. **22**, 103059 (2020).

[47] T. Reimann, A. Bauer, C. Pfleiderer, P. Böni, P. Trtik, A. Tremsin, M. Schulz, and S. Mühlbauer, Neutron diffractive imaging of the skyrmion lattice nucleation in MnSi, Phys. Rev. B **97**, 020406(R) (2018).

[48] T. Lancaster, R. C. Williams, I. O. Thomas, F. Xiao, F. L. Pratt, S. J. Blundell, J. C. Loudon, T. Hesjedal, S. J. Clark, P. D. Hatton *et al.*, Transverse field muon-spin rotation signature of the skyrmion-lattice phase in Cu_2OSeO_3, Phys. Rev. B **91**, 224408 (2015).

[49] J. S. Möller, P. Bonfà, D. Ceresoli, F. Bernardini, S. J. Blundell, T. Lancaster, R. De Renzi, N. Marzari, I. Watanabe, S. Sulaiman *et al.*, Playing quantum hide-and-seek with the muon: localizing muon stopping sites, Phys. Scr. **88**, 068510 (2013).

[50] S. J. Clark, M. D. Segall, C. J. Pickard, P. J. Hasnip, M. J. Probert, K. Refson, and M. C. Payne, First principles methods using CASTEP, Z. Kristallogr. **220**, 567 (2005).

[51] B. M. Huddart, Muon stopping sites in magnetic systems from density functional theory, Ph.D. thesis, Durham University, 2020.

[52] J. P. Perdew, K. Burke, and M. Ernzerhof, Generalized Gradient Approximation Made Simple, Phys. Rev. Lett. **77**, 3865 (1996).

[53] A. Maisuradze, Z. Guguchia, B. Graneli, H. M. Rønnow, H. Berger, and H. Keller, μSR investigation of magnetism and magnetoelectric coupling in Cu_2OSeO_3, Phys. Rev. B **84**, 064433 (2011).

[54] P. Bonfà, I. J. Onuorah, and R. De Renzi, Introduction and a quick look at MUESR, the magnetic structure and mUon embedding site Refinement suite, JPS Conf. Proc. **21**, 011052 (2018).

[55] M. Belesi, T. Philippe, I. Rousochatzakis, H. C. Wu, H. Berger, S. Granville, I. V. Shvets, and J.-P. Ansermet, Magnetic properties of the magnetoelectric compound Cu_2OSeO_3: Magnetization and ^{77}Se NMR study, J. Phys.: Conf. Ser. **303**, 012069 (2011).

[56] S. Seki, S. Ishiwata, and Y. Tokura, Magnetoelectric nature of skyrmions in a chiral magnetic insulator Cu_2OSeO_3, Phys. Rev. B **86**, 060403(R) (2012).

[57] S. L. Zhang, G. van der Laan, and T. Hesjedal, Direct experimental determination of spiral spin structures via the dichroism extinction effect in resonant elastic soft x-ray scattering, Phys. Rev. B **96**, 094401 (2017).

[58] J. D. Bocarsly, C. Heikes, C. M. Brown, S. D. Wilson, and R. Seshadri, Deciphering structural and magnetic disorder in the chiral skyrmion host materials $Co_xZn_yMn_z$ $(x + y + z = 20)$, Phys. Rev. Mater. **3**, 014402 (2019).

[59] K. Karube, J. S. White, D. Morikawa, C. D. Dewhurst, R. Cubitt, A. Kikkawa, X. Yu, Y. Tokunaga, T.-H. Arima, H. M. Rønnow *et al.*, Disordered skyrmion phase stabilized by magnetic frustration in a chiral magnet, Sci. Adv. **4**, eaar7043 (2018).

[60] X. Z. Yu, W. Koshibae, Y. Tokunaga, K. Shibata, Y. Taguchi, N. Nagaosa, and Y. Tokura, Transformation between meron and skyrmion topological spin textures in a chiral magnet, Nature (London) **564**, 95 (2018).

[61] D. L. Schlagel, Y. L. Wu, W. Zhang, and T. A. Lograsso, Chemical segregation during bulk single crystal preparation of Ni–Mn–Ga ferromagnetic shape memory alloys, J. Alloys Compd. **312**, 77 (2000).

[62] J. Kindervater, I. Stasinopoulos, A. Bauer, F. X. Haslbeck, F. Rucker, A. Chacon, S. Mühlbauer, C. Franz, M. Garst, D. Grundler *et al.*, Weak Crystallization of Fluctuating Skyrmion Textures in MnSi, Phys. Rev. X **9**, 041059 (2019).

[63] Durham Collections, doi: 10.15128/r2w9505053g.